



# HI–shielding of H<sub>2</sub> in UV–irradiated protogalaxies: suppression of the photodissociation rate

Meredith Neyer<sup>1,2\*</sup>  and Jemma Wolcott-Green<sup>1</sup> 

<sup>1</sup>*Department of Physics, University of California Santa Barbara, MC 9530, Santa Barbara, CA 93106, USA*

<sup>2</sup>*Department of Physics and Kavli Institute for Astrophysics and Space Research, Massachusetts Institute of Technology, Cambridge, MA 02139, USA*

## ABSTRACT

We study the impact of neutral hydrogen absorption on H<sub>2</sub> photodissociation in protogalactic haloes exposed to soft-UV radiation. Lyman-series absorption can significantly deplete dissociating photons as line overlap with the H<sub>2</sub> Lyman-Werner bands occurs for neutral column densities exceeding 10<sup>22</sup> cm<sup>-2</sup>, but this effect has not been previously included in studies of protogalactic haloes. We use high-resolution three-dimensional hydrodynamic simulations to investigate this “HI–shielding” in three metal-free atomic cooling haloes collapsing at redshift  $z \sim 10 - 20$ . We use CLOUDY modeling to update a previous fitting formula for HI–shielding which is a better model for shielding of non-ground state H<sub>2</sub> rovibrational populations and implement the new fit in our simulations. We find that the inclusion of HI–shielding increases the “critical flux” for suppression of H<sub>2</sub> cooling in these haloes by  $\sim 60 - 100$  per cent. The larger critical flux has implications in particular for the predicted numbers of candidate haloes in which “direct collapse” could seed massive ( $\sim 10^5 M_{\odot}$ ) black holes at  $z \sim 15$ .

**Key words:** cosmology: theory – early Universe – galaxies: formation – molecular processes – stars: Population III

## 1 INTRODUCTION

Molecular hydrogen, H<sub>2</sub>, has been extensively studied in the context of the first generation of stars and galaxies, in which it plays a crucial role as the primary coolant of primordial gas below  $\sim 10^4$  K (for a review, see Bromm & Yoshida 2011). Prior to the production and dispersion of metals by the supernovae, the thermodynamic evolution of pristine primordial gas depends sensitively on the H<sub>2</sub> abundance and therefore on the photodissociation of H<sub>2</sub>, which occurs in the presence of soft UV photons in the “Lyman–Werner” (LW) bands (11.1–13.6 eV).

Depletion of H<sub>2</sub> by LW radiation has been shown to raise the minimum mass of protogalactic haloes in which gas is able to condense and cool, thus delaying star formation in smaller “minihaloes” (Haiman et al. 1997, 2000; Machacek et al. 2001; Yoshida et al. 2003; Mesinger et al. 2006; Wise & Abel 2007; O’Shea & Norman 2008; Kulkarni et al. 2020; ?). In more massive haloes, with virial temperatures  $\gtrsim 10^4$  K, cooling by neutral hydrogen allows gas to condense in haloes even in the absence of significant H<sub>2</sub> cooling, rendering these “atomic cooling haloes” (ACHs) less vulnerable to feedback from a cosmological background LW radiation (e.g. Oh & Haiman 2002). Typically, the column densities of H<sub>2</sub> in ACHs grow large enough that H<sub>2</sub> becomes self-shielding: systematic depletion of LW band photons in the outer layers of the halo depresses photodissociation of H<sub>2</sub> in the core, allow-

ing the gas to cool to temperatures of a few hundred Kelvin. However, sufficiently strong LW radiation fields have been shown to suppress the H<sub>2</sub> abundance and thereby to prevent gas in ACHs from cooling below the virial temperature of the halo (see Inayoshi et al. 2020, and references therein). This threshold LW flux strength is commonly referred to as the critical flux or “ $J_{\text{crit}}$ ” and has been typically found in hydrodynamic simulations to be in the range 10<sup>3–4</sup> in the customary units 10<sup>-21</sup> erg s<sup>-1</sup> cm<sup>-2</sup> Hz<sup>-1</sup> sr<sup>-1</sup>. While this is orders of magnitude larger than the expected cosmological background (e.g. Dijkstra et al. 2008), a collapsing halo near a particularly bright neighboring galaxy with recently-formed Pop III stars may be exposed to a such a flux (Visbal et al. 2014; Regan et al. 2017); in this “synchronized collapse” scenario, if the two collapse within a short period of time – of order a few Myr – the second halo to cross the atomic cooling threshold may have H<sub>2</sub>–cooling entirely suppressed.

The presence of a super-critical flux has implications for the formation of massive seed black holes,  $\sim 10^{(4-5)} M_{\odot}$ ; rapid accretion in ACHs that remain near the virial temperature; these “heavy seeds” could help explain the existence of the earliest supermassive black holes, observed to have masses  $\gtrsim 10^9 M_{\odot}$  at redshifts  $z \gtrsim 6$  and as high as  $\gtrsim 7.5$  (Fan et al. 2001, 2003; Morganson et al. 2012; Mazzucchelli et al. 2017; Wang et al. 2019; Yang et al. 2019; Wang et al. 2021). These heavy seeds are commonly referred to as “direct collapse” black holes, though they’re thought to form via an intermediary supermassive star phase (e.g. Haemmerlé et al. 2018).

Extensive work has been done to constrain the value of

\* E-mail: mneyer@mit.edu; jemma@ucsb.edu

$J_{\text{crit}}$  using hydrodynamic simulations of ACHs, which relies on detailed modeling of the  $\text{H}_2$  chemistry. Since the fraction of haloes exposed to a super-critical UV flux depends sensitively on  $J_{\text{crit}}$ , even small changes in the photodissociation rate significantly alters the predicted prevalence of direct collapse halo candidates (Dijkstra et al. 2008; Ahn et al. 2009; Agarwal et al. 2012; Dijkstra et al. 2014; Chon et al. 2016).

### 1.1 The $\text{H}_2$ photodissociation rate

Self-shielding by  $\text{H}_2$  occurs as the LW bands become optically thick at column densities  $\gtrsim 10^{13} \text{ cm}^{-2}$ , suppressing the photodissociation rate (e.g. Draine & Bertoldi 1996). The optically-thick rate in general depends on the column density, gas temperature, rovibrational populations of  $\text{H}_2$  (Wolcott-Green & Haiman 2019), and details of the incident spectrum (Agarwal & Khochfar 2014; Sugimura et al. 2014; Wolcott-Green et al. 2017), and is prohibitively computationally expensive to calculate on-the-fly in simulations, due to the large number of LW transitions. Simulations most often therefore implement a fitting formula to model the optically-thick rate and rely on local estimates of the column density (Wolcott-Green et al. 2011, but see Hartwig et al. 2015).

In addition to self-shielding, absorption of LW photons by neutral hydrogen Lyman series resonances can decrease the rate of  $\text{H}_2$ -photodissociation. Processing of the cosmological UV background by HI in the pre-reionization IGM has been studied in detail (Haiman et al. 1997, 2000); however, the effects of HI absorption *within* protogalactic halos has not previous been included in 3D simulations. Using one-zone models, Wolcott-Green & Haiman (2011) found that this HI-shielding of  $\text{H}_2$  can significantly decrease the LW photodissociation rate when the column density exceeds  $N_{\text{HI}} \gtrsim 10^{22} \text{ cm}^{-3}$  and provided an analytic fit for the suppression factor  $f_{\text{shield,HI}}$ .

In a study of the escape fraction of LW *out of* ACHs, Schauer et al. (2015) used the WH11 fitting formula to quantify the effect of HI absorption of LW photons emitted stars within the halo. They found the LW escape fraction was reduced by a factor of three, owing to the large neutral column density. In a later study of more massive halos,  $10^{7-8} M_{\odot}$ , Schauer et al. (2017) found a significantly smaller effect, with escape fractions reduced by up to  $\sim 29$  per cent due to HI absorption, possibly due to significantly more ionization by stellar clusters in the haloes resulting in lower neutral column densities. Nevertheless, these results point to the possible importance of HI-shielding of  $\text{H}_2$  in primordial ACHs irradiated by an external LW field.

In this study, we use the three-dimensional hydrodynamic simulation code ENZO to test the effect of absorption by HI on  $J_{\text{crit}}$  in three UV-irradiated protogalaxies collapsing at  $z \sim 10$ . We use a modified version of the WH11 fitting formula for HI-shielding of  $\text{H}_2$  that we updated to better fit non-ground state  $\text{H}_2$  rovibrational populations, which become important at the temperatures and densities of gravitationally collapsing ACHs. Our modified fitting formula, obtained using data for the  $\text{H}_2$  rovibrational populations from CLOUDY, is accurate to within  $\sim 30$  per cent at  $T = 500 - 8000 \text{ K}$ ,  $n = 10^{0-5} \text{ cm}^{-3}$ , and column densities  $N_{\text{HI}} \lesssim 10^{24} \text{ cm}^{-2}$ , and can be easily implemented in chemical models for future studies.

The rest of this paper is organized as follows. In § 2 we

provide details of our simulations and calculations of the HI-shielding; we discuss our results in § 3 and conclude with a summary in § 4.

## 2 NUMERICAL MODELING

### 2.1 Simulations

We run simulations of three atomic cooling halos using ENZO, a publicly-available three-dimensional adaptive mesh refinement (AMR) hydrodynamic code (Bryan et al. 2014). Initial conditions for a box  $1h^{-1} \text{ Mpc}$  on a side and  $128^3$  root grid were generated using MUSIC (Hahn & Abel 2011). In order to select haloes for higher resolution “zoom-in” simulations, we performed an initial dark-matter only ENZO run from  $z = 99$  to  $z = 10$ . We used the ROCKSTAR halo finder package (Behroozi et al. 2013) to identify a halo with mass above the atomic cooling threshold at  $z = 10$ ; we then added three additional levels of refinement using nested grids which enclose the Lagrangian volume for the halo of interest, yielding an effective  $1024^3$  resolution and dark matter particle mass  $\sim 85M_{\odot}$ .

Each halo is then run with + DM “zoom-in” simulations initialized at  $z = 99$  to a maximum refinement level of 18, which results in the highest resolution regions having a minimum cell size of  $.0298h^{-1} \text{ pc}$ . Additional refinement is added each time the baryon or dark matter mass exceeds four times that of the most refined cell. We also imposed that the local Jeans length is resolved by at least 16 cells to prevent spurious fragmentation (Truelove et al. 1997).

We utilize the 9-species non-equilibrium primordial chemistry network within ENZO to model the chemical evolution of the gas. The cooling function from Galli & Palla (1998) is implemented to model the radiative cooling by  $\text{H}_2$ . Several of the reaction rate calculations have been modified in the ENZO chemistry code as described in Wolcott-Green et al. 2021 (see their Appendix A for details). For  $\text{H}_2$  self-shielding, we use the local column density from the “Sobolev-like” method described in WGH11 and their fitting formula for the optically-thick rate.<sup>1</sup> We assume a blackbody incident radiation field at temperature  $T = 10^5 \text{ K}$ .

In order to determine the impact of HI-shielding, we run realizations of each halo to determine the value of  $J_{\text{crit}}$  first with  $\text{H}_2$  self-shielding only, using the Newton-Raphson method to find  $J_{\text{crit}}$ , and then subsequently run each with HI-shielding included, using our new fitting formula § 2.2.

We use the publicly-available package YT (?) for simulation data analysis and visualization<sup>2</sup>. Throughout, we adopt the cosmological parameters from the Planck 2018 collaboration (Planck Collaboration et al. 2018),  $\Omega_{\text{m}} = 0.315$ ,  $\Omega_{\Lambda} = 0.685$ ,  $\Omega_b = 0.0493$ ,  $h = 0.674$ ,  $\sigma_8 = 0.811$ , and  $n = 0.965$ .

<sup>1</sup> This fit has since been updated by Wolcott-Green & Haiman (2019) to account for non-ground state rovibrational populations; however, using the updated fit would not affect our conclusions, since we are interested here in the change in  $J_{\text{crit}}$  due to HI-shielding, rather than the precise value of the critical flux.

<sup>2</sup> yt-project.org

$$\log(N_{\text{H}_2}/\text{cm}^{-2}) = 16, \log(n/\text{cm}^{-3}) = 3$$

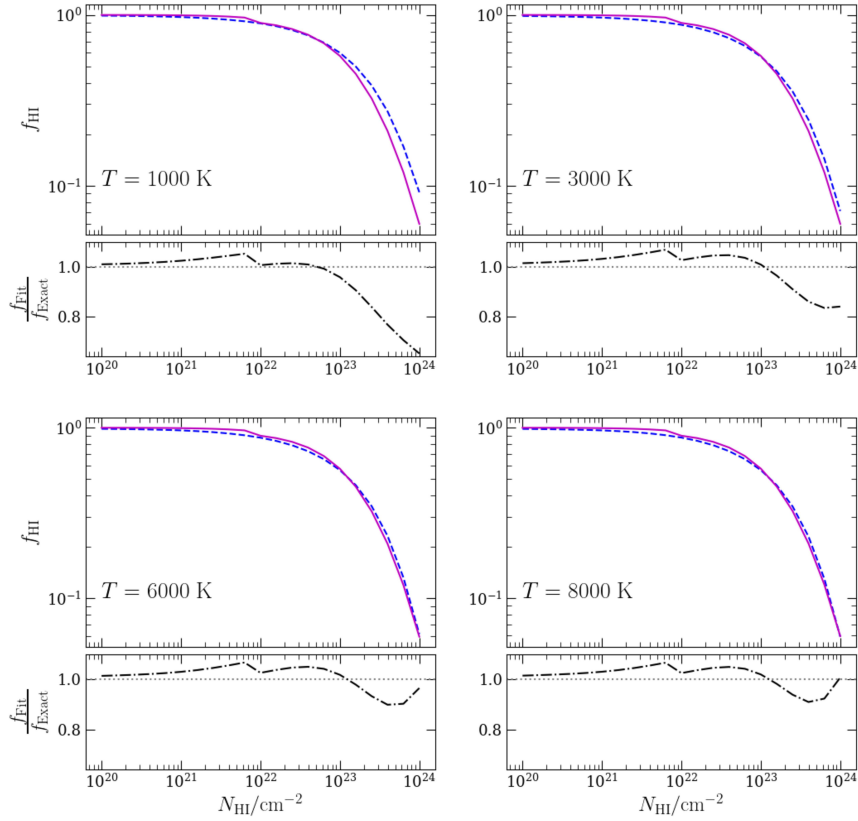


**Figure 1.** The effect of shielding by HI on the H<sub>2</sub> photodissociation rate is parameterized by a shielding factor  $f_{\text{HI}} = k_{\text{diss}}(n, T, N_{\text{H}_2}, N_{\text{HI}})/k_{\text{diss}}(n, T, N_{\text{H}_2})$ . The blue dashed lines show the HI-shielding factor from the full calculation,  $f_{\text{exact}}$ , with CLOUDY-derived rovibrational populations for H<sub>2</sub>. The magenta solid lines show our fit. The black dot-dashed line in each lower panel shows the ratio of our fit to the exact calculation. In order to isolate the HI fitting formula accuracy from that for self-shielding, we calculate  $f_{\text{fit}}$  as  $f_{\text{HI,fit}} \times f_{\text{H}_2,\text{exact}}$ . All are shown for  $\log(n/\text{cm}^{-3}) = 3$ , and  $\log(N_{\text{H}_2}/\text{cm}^{-2}) = 16$ .

## 2.2 HI-shielding of H<sub>2</sub>

In order to find the exact optically-thick photodissociation rate, we use the method described in detail in WGH19 and summarized briefly here. The rate calculation includes contributions from LW transitions originating in the 301 bound rovibrational levels of the electronic ground state. We use the spectral synthesis code CLOUDY (Ferland et al. 2017) to model the H<sub>2</sub> rovibrational populations at  $T = (500-8000)\text{K}$ , densities  $T = 10^{(0-5)} \text{cm}^{-3}$ ,  $N_{\text{HI}} = 10^{(20-25)} \text{cm}^{-2}$ , and  $N_{\text{H}_2} = 10^{(14-17)} \text{cm}^{-2}$ . The fractional populations are then input in the rate calculation for each density and temperature combination.

In order to determine the impact of HI-shielding, the rate is calculated with and without HI Lyman series absorption for each  $n, T, N_{\text{H}_2}$ . We define the dimensionless HI shield factor as:

$$f_{\text{sh,HI}} = \frac{k_{\text{diss}}(n, T, N_{\text{HI}}, N_{\text{H}_2})}{k_{\text{diss}}(n, T, N_{\text{H}_2})}. \quad (1)$$

In order to develop our fit, we began with the form used in WH11,

$$f_{\text{sh,HI}} = \frac{\chi}{(1+x)^\delta} \exp(-\alpha x) \quad (2)$$

which was used in that study for photodissociation of H<sub>2</sub> in the ground rovibrational state only; we modified the parameters using the downhill simplex method AMOEBA provided in Numerical Recipes.

Here,  $x = N_{\text{HI}}/\zeta$  and our best fit parameters are:

$$\alpha = 1.45 \times 10^{-1}$$

$$\delta = 1.5$$

$$\zeta = 2.85 \times 10^{23} \text{cm}^{-2}$$

$$\chi = \begin{cases} 1, & N_{\text{HI}} < 10^{22} \text{cm}^{-2} \\ 0.95, & N_{\text{HI}} \geq 10^{22} \text{cm}^{-2} \end{cases}$$

Figure 1 shows the new HI-shielding factor fit,  $f_{\text{fit}}$  (Equation 2), and the exact shielding factor from the full calculation,  $f_{\text{exact}}$ , at fixed  $\log(n/\text{cm}^{-3}) = 3$ ,  $\log(N_{\text{H}_2}/\text{cm}^{-2}) = 16$  and a range of temperatures. In the lower part of each panel

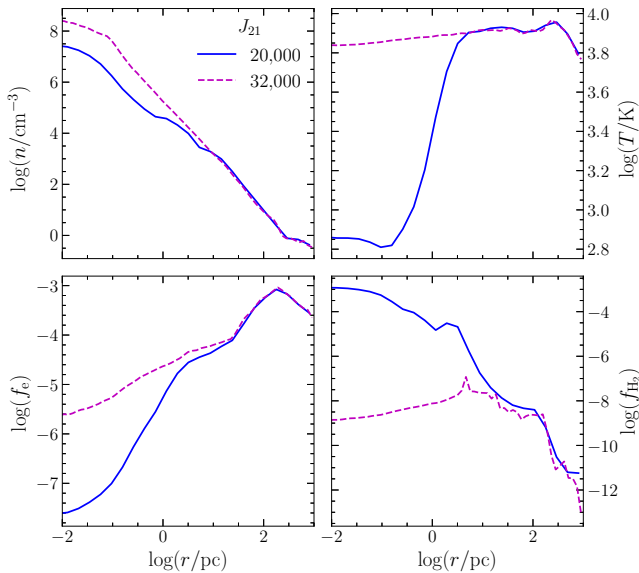


**Figure 2.** Spherically-averaged radial profiles for Halo B at the collapse redshift showing density (upper left), temperature (upper right), electron fraction (lower left), and H<sub>2</sub> fraction (lower right). Lyman-Werner fluxes are  $J_{21} = 20,000$  (sub-critical; blue solid lines) and  $J_{21} = 32,000$  (super-critical; magenta dashed lines). The radial distance is measured in physical units.

**Table 1.** Critical fluxes with and without HI-shielding in  $J_{21}$  units. Virial masses and collapse redshifts indicated for  $J < J_{\text{crit}}$  runs with HI-shielding.

Halo	$M/10^7 M_{\odot}$	$z_{\text{coll}}$	$T_{\text{vir}}/\text{K}$	$J_{\text{crit}}/10^3$	$J_{\text{crit,HI}}/10^3$
A	2.8	13.0	8,296	11	22
B	8.2	10.9	14,418	17	32
C	2.4	18.0	10,231	10	16

is the ratio between  $f_{\text{fit}}$  and  $f_{\text{exact}}$ . The fitting formula for the shielding function of H<sub>2</sub> by HI is robust in the range of temperatures studied here, 500 – 8000K and is accurate to within a factor of two for column densities  $10^{20-24} \text{ cm}^{-2}$ .

### 3 RESULTS

Figure 2 shows spherically-averaged radial profile of density, temperature, electron fraction, and H<sub>2</sub> fraction for Halo A at the collapse redshift. Results for both sub-critical ( $J_{21} = 20,000$ ) and super-critical ( $J_{21} = 32,000$ ) LW fluxes are shown. Our halos follow the well-known behavior of ACHs cooling in the presence of a photodissociating flux: with  $J < J_{\text{crit}}$ , the H<sub>2</sub> fraction in the halo’s dense core reaches  $\sim 10^{-3}$ , the standard “freeze-out” value (Oh & Haiman 2002); H<sub>2</sub> cooling is efficient and the gas temperature falls below  $10^3 \text{ K}$  in the dense core. Irradiation by a super-critical flux results in a suppressed H<sub>2</sub> fraction,  $\sim 10^{-7}$ , and the temperature remains at  $T_{\text{vir}} \sim 10^4 \text{ K}$  throughout the halo.

To determine  $J_{\text{crit}}$ , we run the zoom-in simulations with varied levels of incident  $J_{\text{LW}}$  to find minimum flux that suppress H<sub>2</sub>-cooling and prevents cooling below the virial temperature. The resulting  $J_{\text{crit}}$  values for each of the three haloes are listed in Table 1. We find that the critical flux

with HI-shielding of H<sub>2</sub> is  $\sim 60-100$  percent larger than without HI-shielding. The  $J_{\text{crit},21}$  values without HI-shielding for these halos are within the range  $(10 - 17) \times 10^3$ , comparable to those found in previous studies, and with HI-shielding  $J_{\text{crit},21}$  are within the range  $(16 - 32) \times 10^3$ . Figure 3 shows phase plots for both sub-critical and super-critical fluxes for Halo B at the collapse redshift.

The increase in  $J_{\text{crit}}$  with HI-shielding of H<sub>2</sub> indicates that the neutral column densities are sufficient in these ACHs for Lyman series absorption to be important, which occurs at  $N_{\text{HI}} \gtrsim 10^{22} \text{ cm}^{-2}$  (see Figure 1). In order to verify this, we find the column densities at the critical density<sup>3</sup> by summing along sightlines extending from the densest point of the halo out to a radius of 100 pc. We show a histogram of 25 such sightlines in Figure 4 at the time when the gas in the core has reached at the critical density, just before runaway cooling occurs. (Results are shown here for Halo B and those from the other two halos are similar. We see that indeed the neutral columns have reached the threshold at which HI-shielding becomes significant.

### 4 CONCLUSIONS

In this study, we examined the impact of HI-shielding of H<sub>2</sub> on the thermal evolution of protogalactic atomic cooling haloes exposed to photodissociating UV radiation using three-dimensional hydrodynamic simulations. We find that incorporation of HI-shielding raised the value of the critical flux to suppress H<sub>2</sub>-radiative cooling,  $J_{\text{crit}}$ , by  $\sim 60 - 100\%$  in the three ACHs we studied. This increase may have important implications for the predicted number of candidate halos that could seed massive black holes at  $z \sim 10$  via direct collapse, which is sensitive to the critical flux.

We used an updated fitting formula to model the suppression of H<sub>2</sub> photodissociation by HI, which can be used in future simulations. The modified fitting function is accurate to within  $\sim 30$  per cent at  $T = 500 - 8000 \text{ K}$ ,  $n = 10^{(0-5)} \text{ cm}^{-3}$  and  $N_{\text{HI}} = 10^{(20-24)} \text{ cm}^{-2}$ .

### ACKNOWLEDGMENTS

We thank Zoltán Haiman and S. Peng Oh for helpful discussions during the course of this work. Meredith Neyer acknowledges funding from an Edison STEM summer research program grant at University of California Santa Barbara. This material is based upon work supported by the National Science Foundation under Award No. 1903935. This work used the Extreme Science and Engineering Discovery Environment (XSEDE; allocation TG-PHY200043), which is supported by National Science Foundation grant number ACI-1548562.

### 5 DATA AVAILABILITY

The data underlying this paper will be shared on reasonable request to the corresponding author.

<sup>3</sup> above which, collisional dissociation dominates the total H<sub>2</sub> destruction rate

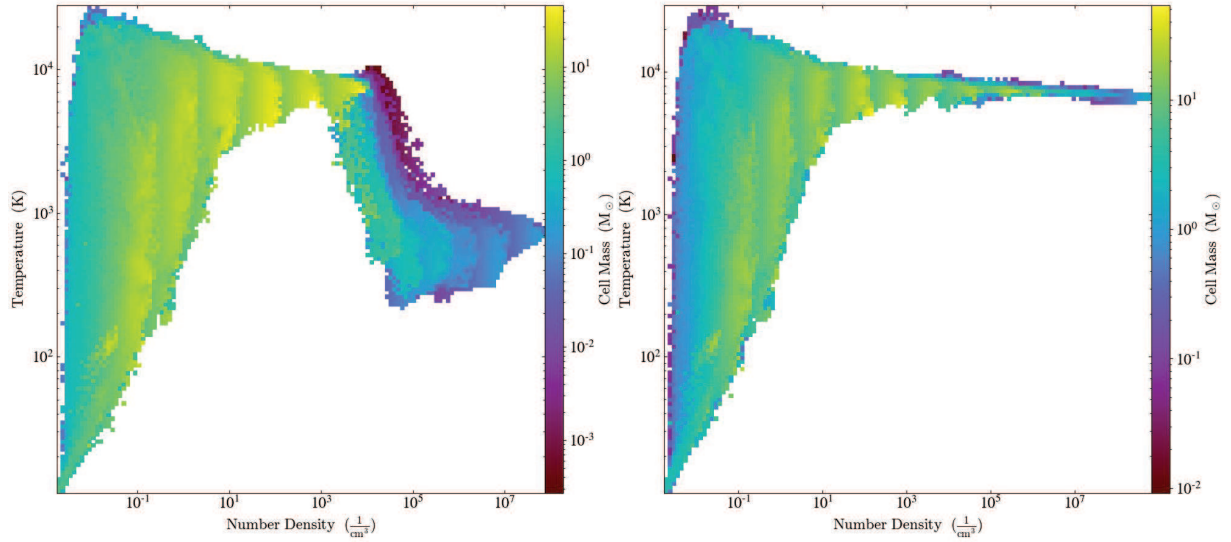


**Figure 3.** Phase plots showing Halo B at the collapse redshift with sub-critical flux (left) and super-critical flux (right).

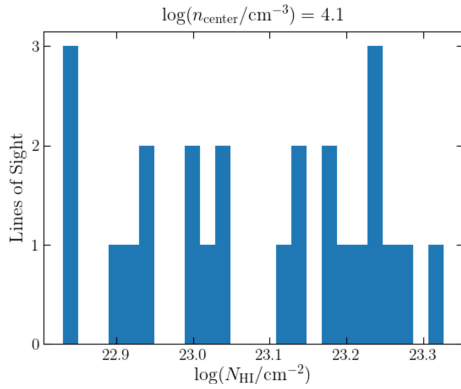


**Figure 4.** Histogram of HI column densities along lines of sight from the center of Halo B just before cooling occurs (sub-critical flux). Column densities exceed the  $N_{\text{HI}} = 10^{22} \text{ cm}^{-2}$  threshold, above which HI-shielding of  $H_2$  becomes significant.

## REFERENCES

- Agarwal B., Khochfar S., 2014, MNRAS, submitted, e-print ArXiv:1407.4115
- Agarwal B., Khochfar S., Johnson J. L., Neistein E., Dalla Vecchia C., Livio M., 2012, MNRAS, 425, 2854
- Ahn K., Shapiro P. R., Iliev I. T., Mellema G., Pen U., 2009, ApJ, 695, 1430
- Behroozi P. S., Wechsler R. H., Wu H.-Y., 2013, ApJ, 762, 109
- Bromm V., Yoshida N., 2011, ARA&A, 49, 373
- Bryan G. L., Norman M. L., O’Shea B. W., Abel T., Wise J. H., Turk M. J., Reynolds D. R., Collins D. C., Wang P., Skillman S. W., 2014, ApJS, 211, 19
- Chon S., Hirano S., Hosokawa T., Yoshida N., 2016, ApJ, 832, 134
- Dijkstra M., Ferrara A., Mesinger A., 2014, MNRAS, 442, 2036
- Dijkstra M., Haiman Z., Mesinger A., Wyithe J. S. B., 2008, MNRAS, 391, 1961
- Draine B. T., Bertoldi F., 1996, ApJ, 468, 269
- Fan X., Narayanan V. K., Lupton R. H., Strauss M. A., Knapp G. R., Becker R. H., White R. L., Pentericci L., Leggett S. K., Haiman Z., Gunn J. E., Ivezić Ž., Schneider D. P., Anderson S. F., Brinkmann J., Bahcall N. A., Connolly A. J., Csabai I., Doi M., Fukugita M., Geballe T., Grebel E. K., Harbeck D., Hennessy G., Lamb D. Q., Miknaitis G., Munn J. A., Nichol R., Okamura S., Pier J. R., Prada F., Richards G. T., Szalay A., York D. G., 2001, AJ, 122, 2833
- Fan X., Strauss M. A., Schneider D. P., Becker R. H., White R. L., Haiman Z., Gregg M., Pentericci L., Grebel E. K., Narayanan V. K., Loh Y.-S., Richards G. T., Gunn J. E., Lupton R. H., Knapp G. R., Ivezić Ž., Brandt W. N., Collinge M., Hao L., Harbeck D., Prada F., Schaye J., Strateva I., Zakamska N., Anderson S., Brinkmann J., Bahcall N. A., Lamb D. Q., Okamura S., Szalay A., York D. G., 2003, AJ, 125, 1649
- Ferland G. J., Chatzikos M., Guzmán F., Lykins M. L., van Hoof P. A. M., Williams R. J. R., Abel N. P., Badnell N. R., Keenan F. P., Porter R. L., Stancil P. C., 2017, Rev. Mex. Astron. Astrofis, 53, 385
- Galli D., Palla F., 1998, A&A, 335, 403
- Haemmerlé L., Woods T. E., Klessen R. S., Heger A., Whalen D. J., 2018, MNRAS, 474, 2757
- Hahn O., Abel T., 2011, MNRAS, 415, 2101
- Haiman Z., Abel T., Rees M. J., 2000, ApJ, 534, 11
- Haiman Z., Rees M. J., Loeb A., 1997, ApJ, 476, 458
- Hartwig T., Glover S. C. O., Klessen R. S., Latif M. A., Volonteri M., 2015, MNRAS, 452, 1233
- Inayoshi K., Visbal E., Haiman Z., 2020, ARA&A, 58, 27
- Kulkarni M., Visbal E., Bryan G. L., 2020, arXiv e-prints, p. arXiv:2010.04169
- Machacek M. E., Bryan G. L., Abel T., 2001, ApJ, 548, 509
- Mazzucchelli C., Bañados E., Venemans B. P., Decarli R., Farina E. P., Walter F., Eilers A. C., Rix H. W., Simcoe R., Stern D., Fan X., Schlafly E., De Rosa G., Hennawi J., Chambers K. C., Greiner J., Burgett W., Draper P. W., Kaiser N., Kudritzki R. P., Magnier E., Metcalfe N., Waters C., Wainscoat R. J., 2017, ApJ, 849, 91
- Mesinger A., Bryan G. L., Haiman Z., 2006, ApJ, 648, 835
- Morganon E., De Rosa G., Decarli R., Walter F., Chambers K., McGreer I., Fan X., Burgett W., Flewelling H., Greiner J., Hodapp K., Kaiser N., Magnier E., Price P., Rix H.-W., Sweeney B., Waters C., 2012, AJ, 143, 142
- Oh S. P., Haiman Z., 2002, ApJ, 569, 558
- Omukai K., 2001, ApJ, 546, 635
- O’Shea B. W., Norman M. L., 2008, ApJ, 673, 14
- Planck Collaboration Aghanim N., Akrami Y., Ashdown M., Aumont J., Baccigalupi C., Ballardini M., Banday A. J.,

- Barreiro R. B., Bartolo N., 2018, A&A, submitted, e-print arXiv:1807.06209
- Regan J. A., Visbal E., Wise J. H., Haiman Z., Johansson P. H., Bryan G. L., 2017, *Nature Astronomy*, 1, 0075
- Schauer A. T. P., Agarwal B., Glover S. C. O., Klessen R. S., Latif M. A., Mas-Ribas L., Rydberg C.-E., Whalen D. J., Zackrisson E., 2017, *MNRAS*, 467, 2288
- Schauer A. T. P., Whalen D. J., Glover S. C. O., Klessen R. S., 2015, *MNRAS*, 454, 2441
- Shang C., Bryan G. L., Haiman Z., 2010, *MNRAS*, 402, 1249
- Sugimura K., Omukai K., Inoue A. K., 2014, *MNRAS*, 445, 544
- Truelove J. K., Klein R. I., McKee C. F., Holliman John H. I., Howell L. H., Greenough J. A., 1997, *ApJL*, 489, L179
- Visbal E., Haiman Z., Bryan G. L., 2014, *MNRAS*, 445, 1056
- Wang F., Yang J., Fan X., Hennawi J. F., Barth A. J., Bañados E., Bian F., Boutsia K., Connor T., Davies F. B., Decarli R., Eilers A.-C., Farina E. P., Green R., Jiang L., Li J.-T., Mazzucchelli C., Nanni R., Schindler J.-T., Venemans B., Walter F., Wu X.-B., Yue M., 2021, *ApJL*, 907, L1
- Wang F., Yang J., Fan X., Wu X.-B., Yue M., Li J.-T., Bian F., Jiang L., Bañados E., Schindler J.-T., Findlay J. R., Davies F. B., Decarli R., Farina E. P., Green R., Hennawi J. F., Huang Y.-H., Mazzucchelli C., McGreer I. D., Venemans B., Walter F., Dye S., Lyke B. W., Myers A. D., Haze Nunez E., 2019, *ApJ*, 884, 30
- Wise J. H., Abel T., 2007, *ApJ*, 671, 1559
- Wolcott-Green J., Haiman Z., 2011, *MNRAS*, 412, 2603
- Wolcott-Green J., Haiman Z., 2019, *MNRAS*, 484, 2467
- Wolcott-Green J., Haiman Z., Bryan G. L., 2011, *MNRAS*, 418, 838
- Wolcott-Green J., Haiman Z., Bryan G. L., 2017, *MNRAS*, 469, 3329
- Wolcott-Green J., Haiman Z., Bryan G. L., 2021, *MNRAS*, 500, 138
- Yang J., Wang F., Fan X., Yue M., Wu X.-B., Li J.-T., Bian F., Jiang L., Bañados E., Beletsky Y., 2019, *AJ*, 157, 236
- Yoshida N., Abel T., Hernquist L., Sugiyama N., 2003, *ApJ*, 592, 645